Article

HT-NMR Studies of the Be−F Coordination Structure in FNaBe and FLiBe Mixed Salts

Jianchao Sun, Hailong Huang, Huiyan Wu, Yushuang Lin, Chengkai Yang,* Min Ge, Yuan Qian, Xiaobin Fu,* and Hongtao Liu*

Read Online

ACCESS | Metrics & More | Article Recommendations | Supporting Information

ABSTRACT: Molten NaF-BeF$_2$ salt is widely considered a promising candidate to replace FLiBe in molten salt reactor applications, which is crucial to reducing the operating costs of the molten salt reactor. Studies on beryllium compounds are rarely conducted due to their volatility and high toxicity. Herein, the Be−F coordination structure of NaF/BeF$_2$ mixed salts was investigated in-depth through various HT-NMR and solid-state NMR methods, which are optimized to be appropriate for the detection of beryllium compounds. It was found that Na$_2$BeF$_4$ and NaBeF$_3$ crystals were transformed into amorphous tetrahedral coordinated networks when there was an increase in the BeF$_2$ concentration in the mixed salts. The main coordinate structure comparisons between FNaBe and FLiBe were analyzed, which exhibit high similarity due to the covalent effect of Be−F bonding, demonstrating the theoretical feasibility of applying FNaBe salts as a substitute for FLiBe in MSR systems. In addition, the transition from the crystal phase to the amorphous phase occurred at a lower BeF$_2$ concentration for FNaBe than that for FLiBe. This was further verified by the results of *ab initio* molecular dynamics (AIMD) simulation that FNaBe melts had more disordered structures, thus causing slight changes in their physical properties.

KEYWORDS: molten salts, ionic structure, high-temperature NMR
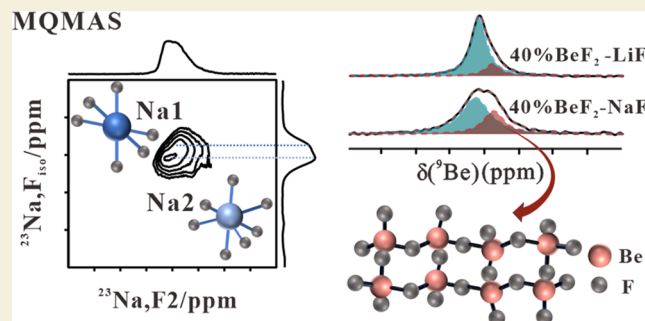
■ INTRODUCTION

With the significant progress of the thorium molten salt reactor (TMSR) system, widespread attention has been paid to it as a novel nuclear energy technology to address the current energy shortages.[1−4] As a major candidate of coolant and fuel salt for TMSR, FLiBe (2LiF-BeF$_2$) demonstrates various advantages, including low melting and high boiling points, high heat capacity and thermal conductivity, high stability under irradiation, as well as excellent neutron performance and high radiation flux.[5] However, the high cost of ^{7}LiF is a realistic constraint on its further commercialization on a large scale. As for the Kairos Power fluoride salt-cooled high-temperature reactor (KP-FHR) system, it is estimated that 1 GWe capacity requires approximately 21−56 t of enriched ^{7}Li.[6] Besides, due to the complex production processes and high costs, it faces economic difficulties for use in power stations for civilian purposes.[7,8] Therefore, it is significant to promote the development of the TMSR system by exploring the solution to replace FLiBe.

As a type of kindred element, NaF possesses highly similar physical properties to LiF, which makes NaF/BeF$_2$ (FNaBe) mixed salts a promising candidate to replace FLiBe in MSR applications.[9,10] Initially, the physical properties of FNaBe melts were studied to explore the feasibility of applying them

as a coolant and fuel salt carrier, with a phase diagram as the main subject of research.[11] The phase diagrams of NaF-BeF$_2$ and NaF-BeF$_2$−UF$_4$ were determined to confirm the applicability of the ternary face system as a liquid medium for transporting nuclear fuel in nuclear reactors.[12] With the development of computational chemistry and numerical simulation methods, many computational methods have been developed to investigate the thermal properties of molten salts, including the soft-sphere equation of state method and first-principles molecular dynamics (FPMD) simulations.[7,13] In addition, the thermal properties of FNaBe, such as thermal conductivity, viscosity, density, and phase transition behavior, were predicted by theoretical calculations.[7] This provides preliminary reference for the design of MSR systems. However, the feasibility of applying FNaBe as a replacement for FLiBe in the MSR systems needs further experimental investigation.
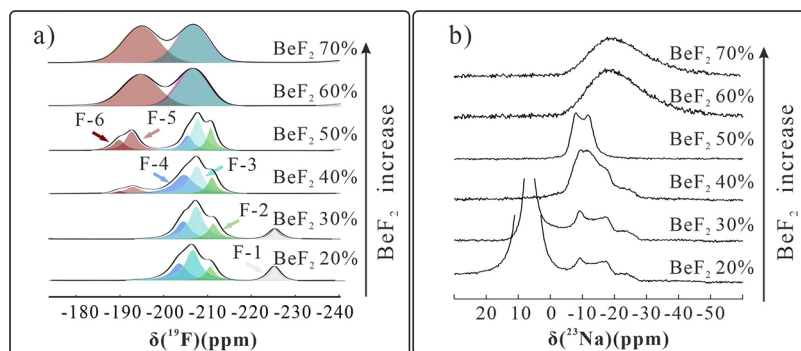
Figure 1. (a) Solid-state ^{19}F MAS NMR spectra and (b) ^{23}Na NMR spectra of FNaBe mixed salts with different BeF$_2$ concentrations.

It is known that the local structure and dynamics of molten salt ions are closely related to their physical properties.[14,15] Therefore, the properties vary with the changes in the chemical composition of the multicomponent molten salt. Understanding the liquid ionic structure plays a crucial role in unraveling the molecular mechanisms behind the physical properties.[16,17] BeF$_2$ is considered to present strong covalent interactions between Be and F, which is similar to SiO$_2$. A complicated coordinate structure and the short-range disordered species will form due to the formation of amorphous constructions, which have specific effects on the properties of beryllium-based compounds. Regarding FLiBe melts, numerous spectroscopic and theoretical studies have been conducted to verify the Be−F bonding structure.[17−21] The results show that a series of beryllium fluoric coordinated species could be formed, and the bonding structures would evolve over a wide range of compositions and temperatures. Raman spectroscopy and NMR measurements were also utilized to explore the formation of the short-range Be−F covalent interaction and the polymeric Be−F units at high BeF$_2$ concentrations.[9,20,22] However, for FNaBe, few similar liquid salt structural studies have been reported. The lack of fundamental research, especially those based on experimentations, hinders the potential use of FNaBe in MSR applications, which is essential for the development of effective coolant components and efficient postprocessing methods for the disposal of nuclear wastes in molten salt reactors.

Nuclear magnetic resonance (NMR) has been proven as an effective and powerful method to examine the microstructure of molten salts, which provides abundant information about both the crystal phase and the amorphous phase.[23,24] In this study, high-temperature NMR (HT-NMR) and solid-state NMR were optimized to prevent the leakage of the samples,[20] which were applied to conduct an in-depth investigation into the chemical bonding structure of NaF/BeF$_2$ binary salts with different component ratios. The chemical shifts and spectral profiles of the ^{19}F, ^{23}Na, and [9]Be NMR signals were investigated. The structure of salt melts and the phase transition process at high temperatures were also checked by HT-NMR. The analytical results confirmed the transformation from the crystal phase to the amorphous phase. Furthermore, the different crystal structures of the mixed salt were investigated by using 2D MQMAS NMR methods such as [23]Na quadrupole interaction fitting. Additionally, a comparison was further made with our previous FLiBe NMR results. The similarity in the main Be−F coordinate structure and the phase transition process illustrates the potential of applying NaF-BeF$_2$ mixed salts as the primary substitute for FLiBe in MSR

applications, although some structural differences still remain. *Ab initio* molecular dynamics (AIMD) calculation was also performed to analyze the structural differences, confirming that Na$^+$ ions promoted the formation of the disordered short-range order and the polymeric units relative to Li$^+$ ions. This provides the necessary considerations to further check the physical properties when the system is used in MSR systems.

■ RESULTS AND DISCUSSION

Local Structure and Structural Transition of FNaBe with Varying Components

NaF/BeF$_2$ mixed salts were synthesized to investigate the local structure of FNaBe, with the BeF$_2$ molar contents ranging from 20% to 70%. ^{19}F solid-state NMR was performed on these salt samples to analyze the ionic structure and spectra, as shown in Figure 1a. Four signals were observed in the spectra of the salt samples with a low BeF$_2$ content (20 and 30% BeF$_2$), which were named F-1 (−224.5 ppm), F-2 (−210.3 ppm), F-3 (−205.7 ppm), and F-4 (−201.9 ppm). The F-1 signal had a similar line type and showed a similar chemical shift with NaF (shown in Figure S1). For this reason, the F-1 signal was assigned to the F-ions of NaF crystals. F-1 signals were detected in the spectra of the salt samples with 20% and 30% BeF$_2$, indicating the presence of an individual NaF crystal phase in the mixed salts with low BeF$_2$ contents. As for the three overlapped signals (F-2, F-3, and F-4), the chemical shifts were different from the ^{19}F NMR signals of NaF or BeF$_2$ (shown in Figure S1). Instead, these signals are quite similar to the ^{19}F NMR signals of crystalline Li$_2$BeF$_4$ reported in our previous works.[9,20,22] XRD patterns of FNaBe salts with 30% or 40% BeF$_2$ (shown in Figure S4) also exhibited characteristic diffraction peaks of different Na−Be−F crystals. Thus, we assigned these overlapped signals to the Na−Be−F crystals, and the diacritical signals suggested the different chemical environments of fluoride ionic coordination. With the increase of BeF$_2$ content, the F-1 signal disappeared from the spectra of 40% BeF$_2$ mixed salts, indicating the absence of an individual NaF crystal phase. In addition, there was little change occurring in the intensity of the three signals (F-2, F-3, and F-4), implying the transition to the crystalline Na−Be−F coordinated structure. This structural transition is discussed in the next section. Furthermore, two new signals emerged at about −191.1 and −187.8 ppm, namely, F-5 and F-6. According to our previous study on FLiBe salts, these two signals can be assigned to the disordered Be−F amorphous structure.[20] With a continual increase in the BeF$_2$ content (above 60% BeF$_2$), only two quite broad signals were observed, which are highly similar to the disordered amorphous Be−F
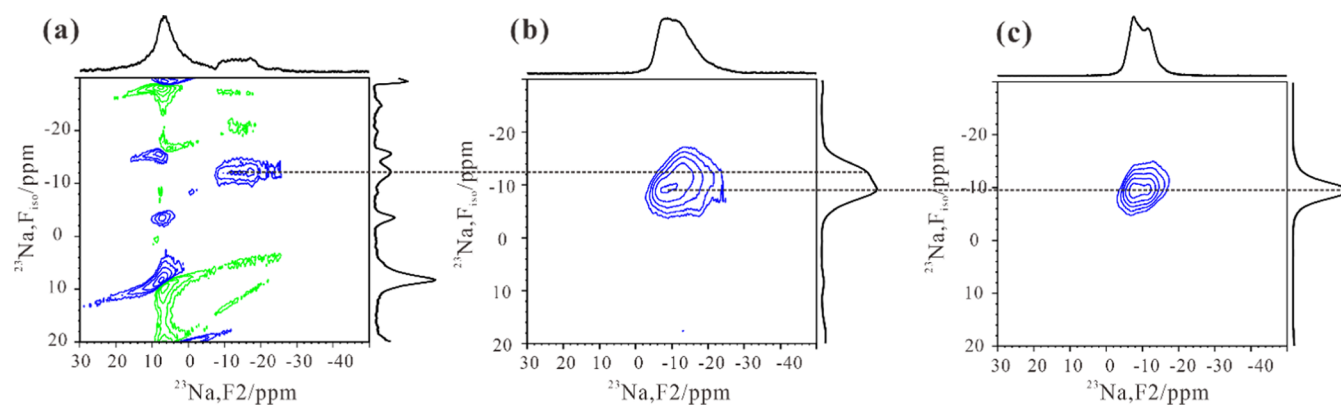
Figure 2. ^{23}Na MQMAS NMR of (a) 30% BeF$_2$−NaF, (b) 40% BeF$_2$−NaF, and (c) 50% BeF$_2$−NaF.
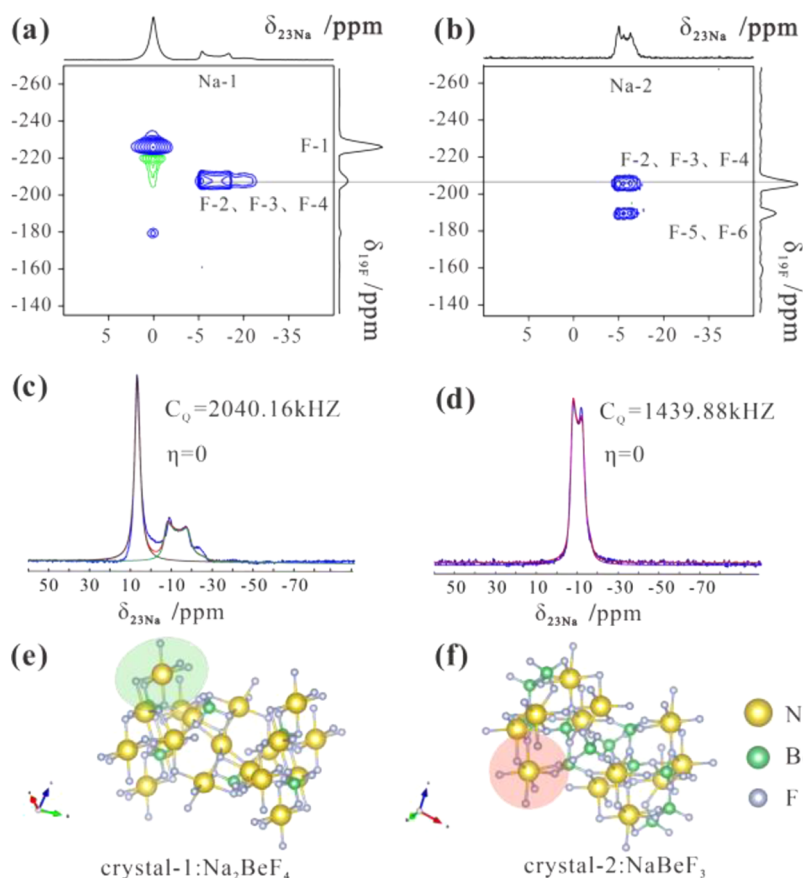
Figure 3. Two-dimensional ^{19}F−^{23}Na HETCOR spectra of FNaBe with (a) 30% BeF$_2$ and (b) 50% BeF$_2$. ^{23}Na experimental and simulated NMR spectra of (c) 30% BeF$_2$−NaF and (d) 50% BeF$_2$−NaF. Structural models of (e) Na$_2$BeF$_4$ and (f) NaBeF$_3$ crystals.

bonding networks. This indicates the completion of structural transition from the crystal phase to the amorphous phase with the increase of BeF$_2$ content. The integration of ^{19}F NMR signals and the intensity curves are shown in Figures S2 and S3, which illustrate the quantitative composition variation during the phase transition. Such a transition from the crystal phase to the amorphous phase could also be verified by X-ray diffraction (XRD), which is shown in Figure S4. Sharp characteristic diffraction peaks of the crystals of the FNaBe samples could be observed, with BeF$_2$ content below 50%, indicating the existence of the crystal phase. When the BeF$_2$ content was further increased above 60%, the diffraction

signals of crystals disappeared, demonstrating the transition of the sample into a completely amorphous state.

^{23}Na solid-state NMR was also performed to examine the structure of the FNaBe mixed salts. Solid-echo pulse sequence was referenced to capture the signals with significant quadrupole interaction with the spectra shown in Figure 1b. Similar to ^{19}F NMR, the signals of NaF and Na−Be−F crystals were detected in the salt samples with low BeF$_2$ contents. With the increase of BeF$_2$ content, only a broad signal was captured, indicating the formation of the amorphous phase. Based on the above results of ^{19}F and ^{23}Na NMR, an overview of the structural changes in solidified FNaBe mixed salts was gained. With the increase of BeF$_2$ content, the NaF crystal phase

disappeared gradually and the NaF-BeF$_2$ coordinated crystal phase developed. When the BeF$_2$ content reached 60%, the crystalline structure vanished entirely, resulting in a transition into amorphous phases.

Crystal Structures of FNaBe Mixed Salts with a Low BeF$_2$ Content

Notably, the line-shape of the crystal signals was clearly different from the BeF$_2$ contents, especially the ^{23}Na signal of the samples with low BeF$_2$ ratios. This indicates the existence of different crystal structures in these samples. However, due to the intense quadrupole interaction of ^{23}Na spins,[25] the amplification of the signals leads to the evident overlap of the line-shape, thus hindering signal decomposition. To resolve signal overlap while obtaining the NMR spectra with high resolution and high sensitivity, the two-dimensional multiple-quantum magic angle spinning (2D MQMAS) method was used for these samples.[26−28] The elimination of second-order quadrupolar broadening significantly increased the resolution of the NMR signals.[29] With control applied on multiquantum excitation, this technique enables the acquisition of details on ^{23}Na NMR signals.

During the MQMAS NMR experiment, the isotropic chemical shift of the quadrupole signals was observed. As for 30% BeF$_2$−NaF salt, two signals were observed in the ^{23}Na spectrum: a narrow signal at 7.1 ppm and a broad signal between −8 and −27 ppm. As shown in Figure 2a, the broad ^{23}Na signals show correlation peaks with only one signal at −12.1 ppm, indicating that this signal is broadened by the strong quadrupole interaction. It can be assigned to the Na−Be−F crystal phase, namely, crystal-1. For the narrow signal at 7.1 ppm, one major cross-peak was observed with the signal at 7.1 ppm in the F1 dimension. Considering the chemical shift, this signal was assigned to the Na$^+$ ions in the NaF crystals. Because of the symmetric octahedral geometry of NaF crystals, the quadrupole interaction was severely suppressed, which led to a narrow line-shape.[30] The strong T$_1$ noise and the poor phase of this signal in the 2D spectra were attributed to the excessively long relaxation and the significant disparity in the intensity between the two signals.

Concerning the 40% BeF$_2$−NaF salt, the signal at 7.1 ppm disappeared from the ^{23}Na spectrum, indicating the absence of NaF crystals. This is consistent with the result of ^{19}F NMR. Besides, the broad signal remained between −8 ppm and −27 ppm, while the line-shape of this signal was barely different from the 30% BeF$_2$−NaF salt. An MQMAS NMR experiment was also performed, and the spectra are shown in Figure 2b. Two cross-peaks were observed at −12.1 ppm (namely, Na-1) and −9.1 ppm (namely, Na-2), indicating that this broad signal is the overlap of two quadrupole signals. By extracting the 1D spectra from the MQMAS spectra, it was found that the line-shape of the signal at −12.1 ppm was highly similar to the broad signal in the 30% BeF$_2$−NaF salt samples. Thus, this signal was assigned to the new crystal-1 phase mixed by NaF-BeF$_2$. As for the signal at −9.1 ppm, this is considered to be another crystal phase that is different from crystal-1. Desirably, this signal was also observed in the spectra of the 50% BeF$_2$−NaF salt sample. For the 50% BeF$_2$−NaF salt, the ^{23}Na signal was reasonably narrowed, and only one cross-peak was observed at about −9.1 ppm. The line-shape and the chemical shift of this signal were highly similar to Na-2 in 40% BeF$_2$−NaF salt. Thus, this Na-2 signal was assigned to the new crystal-2 phase mixed by NaF-BeF$_2$.

The 2D ^{19}F−^{23}Na HETCOR NMR method was performed to verify the crystal structures, and the spectra are shown in Figure 3a,b. As shown in the spectra, both of the ^{23}Na signals of Na-1 (30% BeF$_2$−NaF) and Na-2 (50% BeF$_2$−NaF) have cross-peaks with crystalline ^{19}F signals at about −205 ppm, indicating that these two signals should be different Na−Be−F crystal structures. According to the results of prior studies,[11,31] the NaF-BeF$_2$ mixed salt was predicted to generate two different types of crystals: namely, Na$_2$BeF$_4$ crystals and NaBeF$_3$ crystals. The two ^{23}Na signals revealed by the above NMR results were ascribed to the transition of the crystal structure between these two crystal phases. Quadrupole coupling constants are typically used to infer the deviation from spherical symmetry in the electric fields around atomic nuclei, while asymmetric parameters are commonly used to describe the local symmetry of Na nuclei.[32,33] To verify the signal assignment and crystal structure, the quadrupole interactions between these signals were analyzed in detail. DMfit was used to fit the quadrupole signal simulation of the ^{23}Na NMR signals.[34] According to the simulation results, the Na-1 signal exhibited C_Q = 2040.16 kHz and η = 0, and the Na-2 signal displayed C_Q = 1439.88 kHz and η = 0. The structural models are illustrated in Figure 3e,f. Each Na$^+$ ion was coordinated with six F$^-$ ions in Na$_2$BeF$_4$ crystals,[35] while some of the Na$^+$ ions were coordinated with seven F$^-$ ions in NaBeF$_3$ crystals, with the coordinated structural distortion occurring. As the number of coordinated F$^-$ ions increases in NaBeF$_3$ crystals, there was an increase in the bond distance between F atoms and Na atoms, thus exacerbating the distortion in the specific direction of the coordination electron distribution around Na$^+$ ions. Consequently, the anisotropy of the gradient tensor in the electric field surrounding Na was reduced, thus reducing C_Q.[32] According to the above results, it was verified that Na$_2$BeF$_4$ crystals existed in 30% BeF$_2$−NaF mixed salts and NaBeF$_3$ crystals existed in 50% BeF$_2$−NaF mixed salts.

From the above, it is evident that crystalline structural transition occurred in the solidified mixtures with varying proportions. Specifically, the predominant crystal structure consisted of Na$_2$BeF$_4$ and NaF in 30% BeF$_2$−NaF mixed salts. As the BeF$_2$ content increased to 40%, two distinct Na signals were captured, each of which was ascribed to the crystal structure of Na$_2$BeF$_4$ and NaBeF$_3$, respectively. In the system with 50% BeF$_2$, the primary crystalline structure is NaBeF$_3$ crystals. According to the literature,[20] the strong covalent interactions of Be^{2+} ions can facilitate the coordination between Be^{2+} ions and F$^-$ ions to form BeF$_4^{2-}$ tetrahedral coordinated ions, which has a standard crystal configuration. With the increase of BeF$_2$, the lack of F$^-$ ions led to the formation of more corner-shared F$^-$ ions to keep the tetrahedral coordination. Thus, the NaBeF$_3$ crystal lattice formed when increasing the BeF$_2$ content, which has more corner-shared F$^-$ ions and exhibits some disordered property. Such a transition of crystalline structures was also confirmed by XRD, which is shown in Figure S4. However, this transition of crystal structure was not observed in FLiBe mixed salts during our previous work, in which the LiBeF$_3$ crystal phase was not observed and only the presence of Li$_2$BeF$_4$ crystals was observed. This suggests that the alkali metal ions have a significant effect on the ionic structure of their mixed salts with BeF$_2$.

Amorphous Structure and the Disordered Polymeric Networks of FNaBe Mixed Salts with High BeF$_2$ Content

In ^{19}F and ^{23}Na NMR signals, it was found that the mixed salts with a high BeF$_2$ content were in a state of being completely amorphous. Compared to ^{19}F and ^{23}Na spins, ^{9}Be atoms had a relatively smaller radius, thus leading to the narrower chemical shift distribution.[32,36] Therefore, it was suitable for investigation into the crystalline−amorphous phase transition in the mixed salts. Figure 4 shows the solid-state ^{9}Be MAS NMR
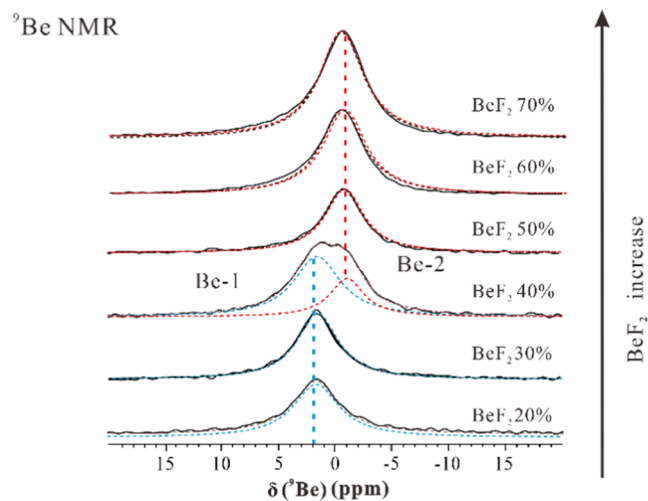

Figure 4. Solid-state ^{9}Be MAS NMR spectra of mixed FNaBe salts with different BeF$_2$ concentrations.

spectra of FNaBe mixed salts with different BeF$_2$ concentrations. There are two signals observed in the spectra, namely, Be-1 and Be-2. The signal variation is quite similar to the FLiBe results in our previous work, indicating the analogous phase transition from the crystal phase into the amorphous phase.[37] According to the above results of ^{19}F and ^{23}Na NMR as well as our previous study on FLiBe, the Be-1 signal can be ascribed to the Be^{2+} ions of the ordered crystal phases and the Be-2 signal can be ascribed to the Be^{2+} ions of the disordered amorphous phases. The distinguishable chemical shifts of Be-1 and Be-2 can be attributed to the abundant corner-sharing tetrahedrally coordinated Be^{2+} cations.

Apparently, the Be-2 signal is the main component when the BeF$_2$ content increases to about 50%, which indicates the formation of the amorphous Be−F networks in the mixed salts. This is clearly different from the results of FLiBe (shown in Figure S5). For FLiBe mixed salts, the Be-2 signal was detected at the BeF$_2$ content of 40% and was gradually enhanced. When the BeF$_2$ content increased to 60%, the Be-2 signal was the main component, suggesting that it is easier to create the disordered Be−F networks in FNaBe mixed salts.[38] That is, Na$^+$ ions are more conducive to the formation of Be−F networks.[16,39] It is implied that the polymeric ions or the network structures in high-temperature FNaBe molten salts are different from FLiBe melts, which causes some difference in their physical properties such as viscosity and heat capacity.[40]

The high-temperature ^{19}F NMR method was performed on FNaBe to investigate the structure of the salt melts. Figure 5 shows the variable-temperature ^{19}F HT-NMR spectra of the FNaBe salt with 50% BeF$_2$. Because the HT-NMR spectra were obtained by static ^{19}F NMR, the resolution of the signals was reduced. Two quite broad signals could be observed at 298
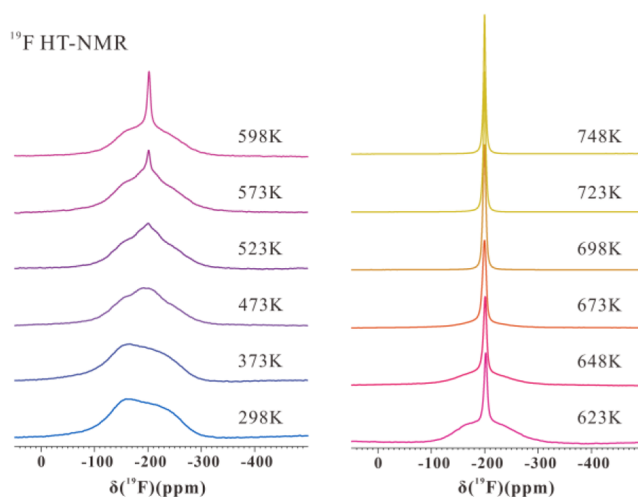
Figure 5. ^{19}F high-temperature NMR spectra of NaF-BeF$_2$ molten salts with 50% concentration of BeF$_2$.

and 373 K, which are still in the solid state. The signal broadening was due to the slow dynamics and the strong dipolar interactions at low temperatures. When the temperature increases to 523 K, a narrow signal at the center of the spectrum appears at −202.1 ppm, and the intensity of this narrow signal enhances gradually, indicating the fast dynamics of these fluorine atoms. According to the phase diagram (shown in Figure S7),[31] the melting point of the 50% FNaBe salt is 649 K. Thus, the fast dynamics of these ^{19}F atoms below the melting point (523 to 623 K) should be due to the enhanced random motion of the amorphous phase. When the temperature increases to quite a high temperature (above 648 K), the intensity of the broad signals decreases and finally a completely narrow signal appears, indicating the melting of the mixed salts. Accompanied by the disappearance of the broad signal, the narrow signal shifts to a low field, which is due to the fast exchange between different species. Such experiments were also performed on FNaBe salts with 40% BeF$_2$ (Figure S6), and a similar variation in the ^{19}F signals could be observed. The HT-NMR results could not provide quantitative structural information. Thus, theoretical simulation would be an efficient method to investigate the structural difference between FNaBe and FLiBe melts.

AIMD simulation was performed to explore the structural differences between FNaBe and FLiBe melts. Figure 6 shows the calculated RDF of FNaBe and FLiBe mixed melts at 900 K with a BeF$_2$ content of 50%. The radial distribution functions (RDFs) of both molten salts indicate both high and narrow peaks (shown in Figure S8), implying high structural stability in both cases. The position of the first peak in the radial distribution function $g(r)$ carries information about the bond length between a central atom and its nearest neighbors.[7] According to the computational results of two different molten salts, the position of the first peak for the F$^−$−F$^−$ ions remained unchanged, without any fluctuation being observed. It is indicated that the average bond length between F$^−$ and F$^−$ ions is identical to that of both FNaBe and FLiBe melts, suggesting the similarity in the main coordinate structure between FNaBe and FLiBe. However, slight differences can still be observed, which will also have some effect on the disordered structure formation. The first peak position for cation−cation Na$^+$−Na$^+$, Li$^+$−Li$^+$, and Be^{2+}−Be^{2+} interactions was notably larger than for F$^−$−F$^−$ interactions, as shown in Figure 6 and S8. This
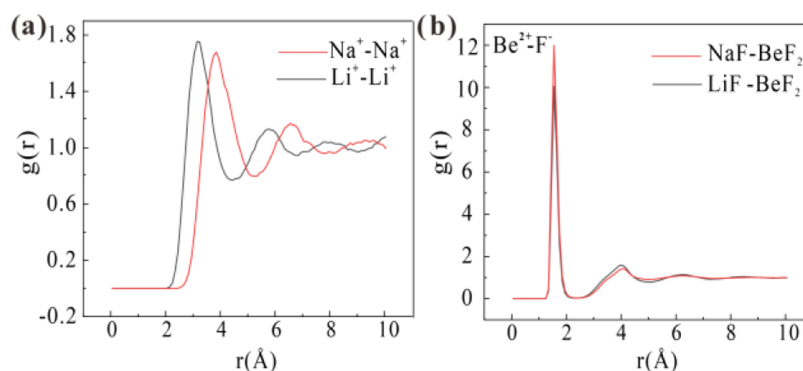
Figure 6. Comparison of the partial radial distribution function of molten FNaBe and FLiBe with 50% BeF_2 content obtained in AIMD simulations at 900 K.

implies a stronger repulsion between cations. The peak intensity indicates the bond strength between ions.[41,42] The average bond length between Na^+−Na^+ ions exceeded that of Li^+−Li^+ ions, with the intensity of the first peak in the RDF being reduced for Na^+−Na^+. These results suggest a higher level of disorder in the motion of Na^+ ions within the FNaBe melt. The weakened interactions should be more beneficial to the formation of the Be−F coordination. Consequently, FNaBe tends to develop irregular networks compared to FLiBe. Figure S8 shows the RDF plots for the Na^+−F^- and Li^+−F^- interactions, highlighting the distinction in the position and intensity of their respective first peaks. Thus, the tendency of FNaBe to form disordered polymeric structures was further verified.

As shown in Figure 6, the interionic distance between the Be^{2+} and F^- ions does not vary significantly. Due to the covalent nature of the Be−F bond, it is difficult to change the bond length.[43,44] In both molten salts, there is barely any change occurring in the bond length for Be^{2+}−F^- and F^-−F^- ions, which are located at 1.55 and 2.59 Å, respectively. It is indicated that the main structure of FNaBe and FLiBe melts is identical, which comprises 4-fold tetrahedron coordination structures of the polymeric Be−F chains/networks in both mixed salts.[7,45] This further underscores the strong covalent interaction of the Be−F bond, which is robust to the change in the alkali metal ions. Notably, the higher first peak intensity of Be^{2+}−F^- in FNaBe indicates the higher strength of the Be−F bond compared to FLiBe. This is suspected to be associated with the tendency of FNaBe to form a network structure more easily.

CONCLUSIONS

In summary, the local structure of NaF/BeF_2 mixed salts and their structural comparisons with LiF/BeF_2 were explored in detail through various NMR methods and AIMD simulation. Both mixed salts exhibit obvious similarity in the main coordinate structure and the phase transition process. Disordered polymeric Be−F chains/networks are formed by 4-fold tetrahedron coordination in FNaBe and FLiBe mixed salts with high BeF_2 contents. This illustrates the potential of applying NaF-BeF_2 mixed salts as the primary substitute for FLiBe in MSR applications. However, alkali metal counterions still have some effect on their local structures. According to the results of ^{19}F, ^{23}Na, and ^{9}Be 1D and 2D NMR experiments, two different crystal structures could be developed in NaF/BeF_2 mixed salts, namely, Na_2BeF_4 and $NaBeF_3$ crystals. Dynamics of the crystalline and amorphous phases during the

phase transition process are also distinguished by in situ HT-NMR. In comparison with FLiBe, the formation of the amorphous phase in FNaBe showed a lower BeF_2 concentration than that of FLiBe. AIMD simulation was performed for both FNaBe and FLiBe, which shows that FNaBe melts possess a more disordered structure. Such differences might lead to the variation in their physical properties such as viscosity, heat capacity, or dissolution capacity of nuclear fuel when using NaF−BeF_2 mixed salts as the coolant and fuel salt, providing a feasible direction to optimizing the properties by adjusting the composition of the mixed salts.

METHODS

Sample Preparation

NaF with a purity of 99.99% was purchased from Sigma-Aldrich. BeF_2 was supplied by the Shanghai Institute of Applied Physics. The purification procedure can be found in a previous work.[46] FNaBe salts were synthesized by the following process. 10 g of the salt was weighed according to the prescribed proportions and mixed in a nickel crucible with a screw cap, which was sealed. Subsequently, the mixture was heated at the rate of 5 °C/min to reach a temperature of 750 °C, where it was held for a duration of 3 h in an electrothermal furnace. Following this, the mixture was cooled to room temperature at the rate of 5 °C/min within the furnace. All of these procedures were conducted within an argon atmosphere glovebox to maintain an inert environment.

X-ray Diffraction

X-ray diffraction measurements were performed on a Bruker D8 ADVANCE using Cu−Kα (1.5406 Å) radiation (35 kV, 25 mA). All samples were mounted on the same sample holder and scanned from $2\theta = 10°$ to $90°$ at a speed of $4°$/min. The experiments were performed at room temperature.

AIMD Simulations

AIMD simulations were performed using the MD software CP2K. A matrix diagonalization procedure was used for the wave-function optimization, and the self-consistent field (SCF) convergence was facilitated by Fermi smearing with the electronic temperature of 900 K. Periodic boundary conditions were set in all three directions. The temperature was kept at 298 K by using NVT system synthesis. The MD time step was set to 0.5 fs with a total time of 15 fs. Only the γ point was used in all calculations. Radial distribution functions and mean square displacement were analyzed by the VMD package.

NMR Experiments

All of the ^{19}F, ^{23}Na, and ^{9}Be NMR experiments were performed on a Bruker AVANCE NEO 400 WB spectrometer operating at 376.61, 105.87, and 56.24 MHz for ^{19}F, ^{23}Na, and ^{9}Be, respectively. A homemade sample container was used to ensure air tightness for all high-temperature NMR experiments performed on a 7.0 mm double-resonance laser-heating HT probe. The experiment temperature was calculated by using the KBr external standard method. The recycle delay was set to 10 s for all of the ^{19}F HT-NMR experiments. For the solid-state NMR experiments at room temperature, a 3.2 mm double-resonance magic angle spinning (MAS) probe was used. For single pulse excitation (SP) NMR experiments, the recycle delay was set to 60 and 30 s for ^{19}F and ^{9}Be, respectively. For the solid-echo pulse sequence, the recycle delay was set to 5 s for ^{23}Na. The spinning rate was set to 20 kHz for ^{19}F and ^{9}Be and to 15 kHz for ^{23}Na. ^{23}Na MQMAS NMR spectra were acquired at a spinning rate of 10 kHz. For ^{19}F–^{23}Na HETCOR NMR experiments, the cross-polarization time was set to 1000 us.[10] The MAS rate was set to 10 kHz. To suppress spin diffusion, FSLG decoupling was applied during t1 (the ^{19}F dimension) and the ^{19}F RF field was set to 100 kHz. Chemical shifts for ^{19}F, ^{23}Na, and ^{9}Be were calibrated using $C_2H_4O_2F_3N$ ($\delta = -74.5$ ppm), a 1 mol/L NaCl aqueous solution ($\delta = 0$ ppm), and solid BeF_2 ($\delta = 0$ ppm), respectively.

■ ASSOCIATED CONTENT

ⓢ Supporting Information

The Supporting Information is available free of charge at https://pubs.acs.org/doi/10.1021/jacsau.4c00177.

> ^{19}F HT-NMR spectra; ^{19}F, ^{23}Na, and ^{9}Be solid-state MAS NMR spectra; XRD patterns; and RDF of AIMD simulations (PDF)

■ AUTHOR INFORMATION

Corresponding Authors

Chengkai Yang — *School of Materials Science and Engineering, Fuzhou University, Fuzhou 350108, China;* ⓞ orcid.org/0000-0001-9868-4831; Email: chengkai_yang@fzu.edu.cn

Xiaobin Fu — *Department of Molten Salt Chemistry and Engineering, Shanghai Institute of Applied Physics, Chinese Academy of Sciences, Shanghai 201800, China; University of Chinese Academy of Sciences, Beijing 100049, China;* ⓞ orcid.org/0000-0002-5005-8134; Email: fuxiaobin@sinap.ac.cn

Hongtao Liu — *Department of Molten Salt Chemistry and Engineering, Shanghai Institute of Applied Physics, Chinese Academy of Sciences, Shanghai 201800, China; University of Chinese Academy of Sciences, Beijing 100049, China;* ⓞ orcid.org/0000-0001-6450-2585; Email: liuhongtao@sinap.ac.cn

Authors

Jianchao Sun — *Department of Molten Salt Chemistry and Engineering, Shanghai Institute of Applied Physics, Chinese Academy of Sciences, Shanghai 201800, China; University of Chinese Academy of Sciences, Beijing 100049, China*

Hailong Huang — *Department of Molten Salt Chemistry and Engineering, Shanghai Institute of Applied Physics, Chinese*

Academy of Sciences, Shanghai 201800, China; ⓞ orcid.org/0000-0003-0924-6720

Huiyan Wu — *Department of Molten Salt Chemistry and Engineering, Shanghai Institute of Applied Physics, Chinese Academy of Sciences, Shanghai 201800, China; University of Chinese Academy of Sciences, Beijing 100049, China*

Yushuang Lin — *School of Materials Science and Engineering, Fuzhou University, Fuzhou 350108, China*

Min Ge — *Department of Molten Salt Chemistry and Engineering, Shanghai Institute of Applied Physics, Chinese Academy of Sciences, Shanghai 201800, China*

Yuan Qian — *Department of Molten Salt Chemistry and Engineering, Shanghai Institute of Applied Physics, Chinese Academy of Sciences, Shanghai 201800, China*

Complete contact information is available at:
https://pubs.acs.org/10.1021/jacsau.4c00177

Author Contributions

X.F. and H.L. conceived and designed the experiments. J.S. and X.F. performed the experiments and analyzed the data. H.H., H.W., and Y.Q. helped synthesize the BeF_2–NaF salts. C.Y., M.G., and Y.L. performed the AIMD simulation. X.F. and J.S. wrote the original manuscript. H.L. helped revise it. All authors proofread the paper, made comments, and approved the manuscript.

Notes

The authors declare no competing financial interest.

■ ACKNOWLEDGMENTS

■ ABBREVIATIONS

FLiBe, LiF–BeF_2; FNaBe, NaF–BeF_2; AIMD, *ab initio* molecular dynamics; HT-NMR, high-temperature nuclear magnetic resonance; TMSR, thorium molten salt reactor nuclear energy system; KP-FHR, Kairos Power fluoride salt-cooled high-temperature reactor; FPMD, first-principles molecular dynamics simulation; MQMAS, multiple-quantum magic angle spinning; HETCOR, heteronuclear correlation spectroscopy; RDF, radial distribution function; SCF, self-consistent field; VMD, visual molecular dynamics; FSLG, frequency switched Lee–Goldberg

■ REFERENCES

(1) Serp, J.; Allibert, M.; Benes, O.; Delpech, S.; Feynberg, O.; Ghetta, V.; Heuer, D.; Holcomb, D.; Ignatiev, V.; Kloosterman, J. L.; et al. The molten salt reactor (MSR) in generation IV: Overview and perspectives. *Prog. Nucl. Energy* **2014**, *77*, 308–319.

(2) Uhlíř, J. Chemistry and technology of Molten Salt Reactors - history and perspectives. *J. Nucl. Mater.* **2007**, *360* (1), 6–11.

(3) Williams, D. F.; Clarno, K. T. Evaluation of salt coolants for reactor applications. *Nucl. Technol.* **2008**, *163* (3), 330–343.

(4) Mallapaty, S. China prepares to test thorium-fuelled nuclear reactor. *Nature* **2021**, *597* (7876), 311–312.

(5) Britsch, K.; Anderson, M. A Critical Review of Fluoride Salt Heat Transfer. *Nucl. Technol.* **2020**, *206* (11), 1625–1641.

(6) Ault, T.; Brozek, K.; Fan, L.; Folsom, M. Lithium Isotope Enrichment: Feasible Domestic Enrichment Alternatives *Dep. Nucl. Eng. Univ. Calif.*, 2012.

(7) Liu, M. M.; Li, X. J.; Xu, T. R.; Yan, L. M.; Tang, Z. F. Mapping relationships between cation-F bonds and the heat capacity, thermal conductivity, viscosity of molten NaF-BeF$_2$. *J. Mol. Liq.* **2022**, *354*, 118915.

(8) Symons, E. A. Lithium Isotope Separation: A Review of Possible Techniques. *Sep. Sci. Technol.* **1985**, *20* (9−10), 633−651.

(9) Liu, Y. Y.; Lan, R. S.; Dong, C. W.; Wang, K.; Fu, X. B.; Liu, H. T.; Qian, Y.; Wang, J. Q. High-Temperature Magic-Angle Spin Nuclear Magnetic Resonance Reveals Sodium Ion-Doped Crystal-Phase Formation in FLiNaK Eutectic Salt Solidification. *J. Phys. Chem. C* **2021**, *125* (8), 4704−4709.

(10) Wu, H. Y.; Huang, H. L.; Cao, L. Z.; Liu, Y. Y.; Dai, J. X.; Ren, C. L.; Ge, M.; Qian, Y.; Hu, S. X.; Fu, X. B.; et al. Probing the Structure and Dynamics of Na plus Ionic Doped LiF Crystals in Fluoride Eutectic Salt by Solid-State NMR. *J. Phys. Chem. C* **2023**, *127* (6), 3093−3098.

(11) Roy, D. M.; Roy, R.; Osborn, E. F. Phase Relations and Structural Phenomena in the Fluoride-Model Systems LiF-BeF$_2$ and NaF-BeF$_2$. *J. Am. Ceram. Soc.* **1950**, *33* (3), 85−90.

(12) Eichelberger, J. F.; Hudgens, C. R.; Jones, L. V.; Pish, G.; Rhinehammer, T. B.; Tucker, P. A.; Wittenberg, L. J. Phase Equilibria for the Ternary Fused-Salt System NaF−BeF$_2$−UF$_4$. *J. Am. Ceram. Soc.* **1963**, *46* (6), 279−283.

(13) Griffard, C.; Penoncello, S. G.; Crepeau, J. C. Use of the Soft-Sphere Equation of State to predict the thermodynamic properties of the molten salt mixtures LiF-BeF$_2$, NaF-BeF$_2$, and KF-BeF$_2$. *Prog. Nucl. Energy* **2013**, *68*, 188−199.

(14) Smith, A. L. Structure-property relationships in actinide containing molten salts - A review: Understanding and modelling the chemistry of nuclear fuel salts. *J. Mol. Liq.* **2022**, *360*, 119426.

(15) Chahal, R.; Roy, S.; Brehm, M.; Banerjee, S.; Bryantsev, V.; Lam, S. T. Transferable Deep Learning Potential Reveals Intermediate-Range Ordering Effects in LiF-NaF-ZrF$_4$ Molten Salt. *JACS Au* **2022**, *2* (12), 2693−2702.

(16) Pauvert, O.; Salanne, M.; Zanghi, D.; Simon, C.; Reguer, S.; Thiaudière, D.; Okamoto, Y.; Matsuura, H.; Bessada, C. Ion Specific Effects on the Structure of Molten AF-ZrF$_4$ Systems (A$^+$ = Li$^+$, Na$^+$, and K$^+$). *J. Phys. Chem. B* **2011**, *115* (29), 9160−9167.

(17) Liu, S. T.; Su, T.; Cheng, J. H.; An, X. H.; Zhang, P.; Liu, H. T.; Yao, S. D.; Xie, L. D.; Hou, H. Q. Investigation on molecular structure of molten Li$_2$BeF$_4$ (FLiBe) salt by infrared absorption spectra and Density Functional Theory (DFT). *J. Mol. Liq.* **2017**, *242*, 1052−1057.

(18) Lam, S. T.; Li, Q.-J.; Ballinger, R.; Forsberg, C.; Li, J. Modeling LiF and FLiBe Molten Salts with Robust Neural Network Interatomic Potential. *ACS Appl. Mater. Interfaces* **2021**, *13* (21), 24582−24592.

(19) Attarian, S.; Morgan, D.; Szlufarska, I. Thermophysical properties of FLiBe using moment tensor potentials. *J. Mol. Liq.* **2022**, *368*120803.

(20) Fu, X. B.; Liu, Y. Y.; Huang, H. L.; Wu, H. Y.; Sun, J. C.; Han, L.; Ge, M.; Qian, Y.; Liu, H. T. Probing the local structure of FLiBe melts and solidified salts by *in situ* high-temperature NMR. *Phys. Chem. Chem. Phys.* **2023**, *25* (29), 19446−19452.

(21) Rodriguez, A.; Lam, S.; Hu, M. Thermodynamic and Transport Properties of LiF and FLiBe Molten Salts with Deep Learning Potentials. *ACS Appl. Mater. Interfaces* **2021**, *13* (46), 55356−55368.

(22) Toth, L. M.; Boyd, G. E.; Bates, J. B. Raman spectra of Be$_2$F$_7$$^{3-}$ and higher polymers of beryllium fluorides in the crystalline and molten state. *J. Phys. Chem. A* **1973**, *77* (2), 216−221.

(23) Huiyan, W.; Junheng, Y.; Yiyang, L.; Hailong, H.; Min, G.; Yuan, Q.; Xiaobin, F.; Hongtao, L. In-situ high-temperature NMR spectroscopy and its applications in molten salt ionic structure studies. *Nucl. Sci. Tech.* **2023**, *46* (03), 113−120.

(24) Rongshan, L.; Yiyang, L.; Xiaobin, F.; Hongtao, L.; Yuan, Q. Probing the glass transition structure of ZrF$_4$-FLiNaK by solid-state MAS NMR. *Nucl. Sci. Tech.* **2021**, *44* (07), 48−54.

(25) Xue, X. Y.; Stebbins, J. F. ^{23}Na NMR chemical shifts and local Na coordination environments in silicate crystals, melts and glasses. *Phys. Chem. Miner.* **1993**, *20* (5), 297−307.

(26) Paul, G.; Bisio, C.; Braschi, I.; Cossi, M.; Gatti, G.; Gianotti, E.; Marchese, L. Combined solid-state NMR, FT-IR and computational studies on layered and porous materials. *Chem. Soc. Rev.* **2018**, *47* (15), 5684−5739 Review.

(27) Medek, A.; Harwood, J. S.; Frydman, L. Multiple-quantum magic-angle spinning NMR: A new method for the study of quadrupolar nuclei in solids. *J. Am. Chem. Soc.* **1995**, *117* (51), 12779−12787.

(28) Laws, D. D.; Bitter, H. M. L.; Jerschow, A. Solid-state NMR spectroscopic methods in chemistry. *Angew. Chem., Int. Ed.* **2002**, *41* (17), 3096−3129.

(29) Graham, T. R.; Nienhuis, E. T.; Reynolds, J. G.; Marcial, J.; Loring, J. S.; Rosso, K. M.; Pearce, C. I. Sodium site occupancy and phosphate speciation in natrophosphate are invariant to changes in NaF and Na$_3$PO$_4$ concentration. *Inorg. Chem. Front.* **2022**, *9* (19), 4864−4875.

(30) Wu, X.; Fronczek, F. R.; Butler, L. G. Structure of LiNO$_3$: point charge model and sign of the ^{7}Li quadrupole coupling constant. *Inorg. Chem.* **1994**, *33* (7), 1363−1365.

(31) Roy, D. M.; Roy, R.; Osborn, E. F. Fluoride Model Systems: III, The System NaF−BeF$_2$ and the Polymorphism of Na$_2$BeF$_4$ and BeF$_2$. *J. Am. Ceram. Soc.* **1953**, *36* (6), 185−190.

(32) Paterson, A. L.; Hanson, M. A.; Werner-Zwanziger, U.; Zwanziger, J. W. Relating ^{139}La Quadrupolar Coupling Constants to Polyhedral Distortion in Crystalline Structures. *J. Phys. Chem. C* **2015**, *119* (45), 25508−25517.

(33) Michaelis, V. K.; Kroeker, S. ^{73}Ge Solid-State NMR of Germanium Oxide Materials: Experimental and Theoretical Studies. *J. Phys. Chem. C* **2010**, *114* (49), 21736−21744.

(34) Massiot, D.; Fayon, F.; Capron, M.; King, I.; Le Calvé, S.; Alonso, B.; Durand, J. O.; Bujoli, B.; Gan, Z. H.; Hoatson, G. Modelling one- and two-dimensional solid-state NMR spectra. *Magn. Reson. Chem.* **2002**, *40* (1), 70−76.

(35) Deganello, S. Diffraction of monochromatic and filtered radiation by γ Na$_2$BeF$_4$ as recorded by precession photography. *Z. Kristallogr.* **1972**, *136* (1−2), 89−97.

(36) Bryce, D. L.; Wasylishen, R. E. Beryllium-9 NMR Study of Solid Bis(2,4-pentanedionato-O,O′)beryllium and Theoretical Studies of ^{9}Be Electric Field Gradient and Chemical Shielding Tensors. First Evidence for Anisotropic Beryllium Shielding. *J. Phys. Chem. A* **1999**, *103* (36), 7364−7372.

(37) Bekiş, D. F.; Thomas-Hargreaves, L. R.; Berthold, C.; Ivlev, S. I.; Buchner, M. R. Structure and spectroscopic properties of etherates of the beryllium halides. *Z. Naturforsch. (B)* **2023**, *78* (3−4), 165−173.

(38) Sen, S.; Yu, P. Observation of a stuffed unmodified network in beryllium silicate glasses with multinuclear NMR spectroscopy. *Phys. Rev. B* **2005**, *72* (13), 132203.

(39) Guo, X. J.; Qian, H. L.; Dai, J. X.; Liu, W. H.; Hu, J. T.; Shen, R. F.; Wang, J. Q. Theoretical evaluation of microscopic structural and macroscopic thermo-physical properties of molten AF-ThF$_4$ systems (A = Li$^+$, Na$^+$ and K$^+$). *J. Mol. Liq.* **2019**, *277*, 409−417.

(40) Salanne, M.; Madden, P. A. Polarization effects in ionic solids and melts. *Mol. Phys.* **2011**, *109* (19), 2299−2315.

(41) Sukhomlinov, S. V.; Müser, M. H. Determination of accurate, mean bond lengths from radial distribution functions. *J. Chem. Phys.* **2017**, *146* (2), 024506.

(42) Bu, M.; Liang, W. S.; Lu, G. M.; Yu, J. G. Static and dynamic ionic structure of molten CaCl$_2$ via first-principles molecular dynamics simulations. *Ionics* **2021**, *27* (2), 771−779.

(43) Dai, J. X.; Han, H.; Li, Q. N.; Huai, P. First-principle investigation of the structure and vibrational spectra of the local structures in LiF-BeF$_2$ Molten Salts. *J. Mol. Liq.* **2016**, *213*, 17−22.

(44) Salanne, M.; Simon, C.; Turq, P.; Heaton, R. J.; Madden, P. A. A first-principles description of liquid BeF$_2$ and its mixtures with LiF: 2. Network formation in LiF-BeF$_2$. *J. Phys. Chem. B* **2006**, *110* (23), 11461−11467.

(45) Smith, A. L.; Capelli, E.; Konings, R. J. M.; Gheribi, A. E. A new approach for coupled modelling of the structural and thermo-physical

properties of molten salts. Case of a polymeric liquid LiF-BeF$_2$. *J. Mol. Liq.* **2020**, *299*, 112165.

 (46) Shaffer, J. H. *Preparation and Handling of Salt Mixtures for the Molten Salt Reactor Experiment.* ORNL-4616; United States, 1971.